International Journal of Solids and Structures 45 (2008) 4756–4765

Contents lists available at ScienceDirect

International Journal of Solids and Structures

journal homepage: www.elsevier.com/locate/ijsolstr

An extended finite element method for modeling near-interfacial crack propagation in a layered structure

Yuhai Yan, Si-Hwan Park *

Department of Civil and Environmental Engineering, University of Hawaii at Manoa, Honolulu, HI 96822, USA

ARTICLE INFO

Article history:
Received 4 October 2007
Received in revised form 20 January 2008
Available online 29 April 2008

Keywords:
Near-interfacial fracture
Extended finite element method
Crack propagation
Layered structure

ABSTRACT

The extended finite element method (XFEM) is applied for the simulation of near-interfacial crack propagation in a metal–ceramic layered structure. An experimental evidence indicates that, in a ceramic–metal–ceramic sandwich structure, a near-interfacial crack in the ceramic layer can be drawn to or deflect away from the metal layer depending on the difference in elastic properties across the interface. To model near-interfacial fracture, only the Heaviside functions are used for the XFEM, and the vector level set method is employed for efficient evaluation of the enrichment functions. The crack propagation paths predicted by the XFEM simulation are found to be consistent with the experimental observation.

1. Introduction

Design of composite structures in many important industrial applications requires good understanding of the fracture behavior near the bi-material interfaces. For example, it has become a widespread practice to strengthen reinforced or prestressed concrete structures with externally bonded fiber-reinforced plastic (FRP) plates. Such a practice has been spurred by FRP's high stiffness-to-weight ratio, strength-to-weight ratio and durability as compared with other conventional materials (Triantafillou and Antonopoulos, 2000). However, the failure mechanism of the strengthened system has not been understood very well, and has been the subject of extensive experimental and analytical studies in the recent past (Büyüköztürk et al., 2004; Camata et al., 2007; Chen and Teng, 2003; Leung, 2006). Among other failure mechanisms, a greater attention is being paid to debonding failure, that is, debonding of the FRP plate from the concrete substrate. A prevalent failure mode in FRP-strengthened systems, debonding failure tends to be highly brittle and thus must be prevented by adequate design (Büyüköztürk et al., 2004). Debonding is a fracture phenomenon that occurs near or on the interface between two distinct materials. As such, relative elastic properties of the constituent materials inevitably affect the fracture process, which makes it harder to predict the crack propagation path.

Numerical methods for simulating crack propagation can be categorized into the discrete inter-element crack approach (Ngo and Scordelis, 1967), embedded discontinuity approach (Simo et al., 1993; Jirásek, 2000), and the extended finite element method (XFEM) (Moës et al., 1999). In the discrete inter-element crack approach a crack is modeled by introducing a separation between element edges when a crack initiation criterion is met. The discrete crack approach is most appropriate when the crack path is known in advance, such as in pure mode I fracture. In general, however, the crack path must be determined by the simulation, and to track an arbitrary crack path the discrete approach requires remeshing and a continuous change in nodal connectivity, which can be quite cumbersome to implement.

* Corresponding author. Tel.: +1 808 956 4249; fax: +1 808 956 5014.
E-mail address: sihwan@hawaii.edu (S.-H. Park).

0020-7683/$ - see front matter © 2008 Elsevier Ltd. All rights reserved.
doi:10.1016/j.ijsolstr.2008.04.016

In both the embedded discontinuity approach and the XFEM, a crack can reside in the interior of a finite element and grow arbitrarily without regard to the mesh topology. The embedded discontinuity approach employs the displacement field consisting of the regular continuous component and the enhanced component containing a discontinuity across the crack. The enriched degrees of freedom associated with discontinuities are eliminated by condensation. In the XFEM, on the other hand, special functions are added to the finite element approximation under the framework of partition of unity (Melenk and Babuška, 1996). To model cracks, the Heaviside function and linear elastic asymptotic crack-tip displacement fields are used (Moës et al., 1999) although only the Heaviside function is used in other implementations (Zi and Belytschko, 2003). A comparative study of the two methods (Jirásek and Belytschko, 2002) shows that the XFEM has advantages over the embedded discontinuity approach in representing kinematic properties and possesses better numerical robustness.

In this study, the XFEM combined with the level set method (LSM) (Osher and Sethian, 1988) is used to simulate the near-interfacial fracture behavior of layered composite structures. The XFEM is capable of modeling crack growth without remeshing and possesses advantages over conventional methods as discussed above. The LSM, on the other hand, is capable of handling the motion of an interface, such as a propagating crack. The combined use of the LSM and XFEM can thus greatly simplify the algorithm to model the crack geometry in three dimensions. The LSM is implemented in the current study which is restricted to plane problems so that methodologies can be readily extended in the future to a three-dimensional setting. We use the vector LSM (Ventura et al., 2003), a version of the LSM specifically tailored toward modeling evolving crack geometries, to evaluate XFEM enrichment functions efficiently.

Among the many XFEM formulations available in the literature, the approach proposed by Zi and Belytschko (2003) does not rely on the use of special crack-tip enrichment functions, so that the partition of unity holds in the entire enriched domain. Chessa et al. (2003) report that the accuracy can be impaired when partially enriched elements are created around the crack-tip by using the crack-tip enrichment functions. The XFEM has been applied to a number of problems in fracture mechanics including channel cracking (Huang et al., 2003) and bi-material interface cracks (Sukumar et al., 2004), but few studies have been reported on near-interfacial cracking. The present study is concerned with the application of the XFEM based on the formulation of Zi and Belytschko (2003) to the simulation of crack growth in layered composite structures, with particular emphasis on the XFEM's capability in predicting the crack path in near-interfacial fracture.

In what follows, we first briefly describe the numerical technique, the XFEM combined with the vector LSM. A pilot problem on the computation of stress intensity factors (SIF) for cracks in a plate under uniaxial loading is then considered to verify the implementation. Numerical simulation of near-interfacial crack propagation in a metal–ceramic layered structure follows and the computed crack paths are compared with experimental results. The paper is concluded by a summary of the results and recommendations for future research.

2. Numerical techniques

2.1. Extended finite element method

The extended finite element method (XFEM) is a numerical technique for modeling discontinuities by local enrichment functions in the area of interest. For the sake of subsequent discussion, let us consider a solid body occupying the domain Ω and containing a crack Γ_c (Fig. 1). In the XFEM formulation by Moës et al. (1999), two types of enrichment, that is, the Heaviside and crack-tip enrichment are included to represent the displacement jump across the crack and the singular near-tip displacement field around the crack-tip. In the present study, we follow Chen (2003) and Zi and Belytschko (2003), who employed the Heaviside enrichment only. Dropping crack-tip enrichment functions eliminates the partially enriched elements on which the partition of unity does not hold, thus avoiding the degradation of accuracy in those elements (Chessa et al., 2003).

The enriched interpolation function for the displacement is written as

$$\mathbf{u}(\mathbf{x}) = \sum_{\mathrm{I}\in N_{\mathrm{f}}} N_{\mathrm{I}}(\mathbf{x})\mathbf{u}_{\mathrm{I}} + \sum_{\mathrm{I}\in N_{\mathrm{h}}} N_{\mathrm{I}}(\mathbf{x})(H(\mathbf{x}) - H(\mathbf{x}_{\mathrm{I}}))\mathbf{a}_{\mathrm{I}}, \tag{1}$$

where $N_{\mathrm{I}}(\mathbf{x})$ is the standard interpolation function used in conventional finite elements and $H(\mathbf{x})$ the Heaviside function. $\mathbf{u}_{\mathrm{I}}$ and $\mathbf{a}_{\mathrm{I}}$ are, respectively, the standard displacement degree of freedom and the enriched degree of freedom associated with

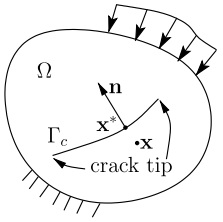

Fig. 1. Domain Ω of a solid body containing a crack Γ_c.

the Heaviside enrichment. N_t is the set of total nodes whereas the set N_h contains the nodes of the elements cut by the crack Γ_c. $H(\mathbf{x})$ is defined as

$$H(\mathbf{x}) = \begin{cases} 1 & \text{if } (\mathbf{x}-\mathbf{x}^*)\cdot\mathbf{n} \geqslant 0 \\ -1 & \text{otherwise} \end{cases}, \tag{2}$$

where $\mathbf{x}^*$ is the closest point to $\mathbf{x}$ on the crack and $\mathbf{n}$ is the unit outward normal to the crack at $\mathbf{x}^*$ (Fig. 1).

The discontinuity due to the Heaviside enrichment functions is illustrated in Fig. 2 for the one-dimensional case, where the whole domain Ω is divided into Ω_- and Ω_+ by the discontinuity at point D. Since only the element connected to nodes 2 and 3 contains the discontinuity, only those nodes are the members of N_h and need to be enriched. The resulting enrichment functions along with the standard shape functions are shown in Fig. 2. A simple calculation reveals that the discontinuity in the displacement is $2N_2(x_D)a_2 + 2N_3(x_D)a_3$. It is clearly seen that the enrichment is local and restricted to the element containing the discontinuity only.

Three-node triangular elements are used exclusively in our implementation for two-dimensional situations, for which more elaborate considerations are necessary since an element can be cut by a crack either completely or partially. For an element that is completely cut by a crack, all the nodes of the element are enriched. An element that is partially cut by a crack contains the crack-tip in its interior. For such an element, the nodes on the edge toward which the crack is heading are not enriched and only the remaining node is enriched. Fig. 3 shows enriched nodes for a two-dimensional structured mesh. See Zi and Belytschko (2003) for a detailed description of the enrichment algorithm.

For elements cut by a crack, the standard Gauss quadrature is not adequate due to discontinuities that exist inside the elements (Sukumar and Prévost, 2003). To accurately evaluate the integrals resulting from the virtual work statement, we divide the element domain into subdomains of triangular shape and then apply a quadrature formula to each subdomain. Depicted also in Fig. 3 is how elements completely cut by a crack and a crack-tip element are partitioned into triangles (shown as dotted lines). In the crack-tip element, a partition touches the crack-tip thus accurately representing the crack-tip position.

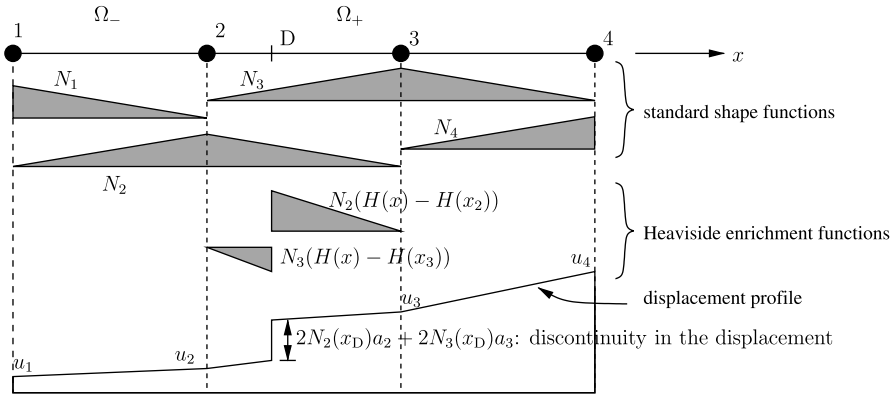

Fig. 2. Representation of a discontinuity by Heaviside enrichment functions: one-dimensional case.

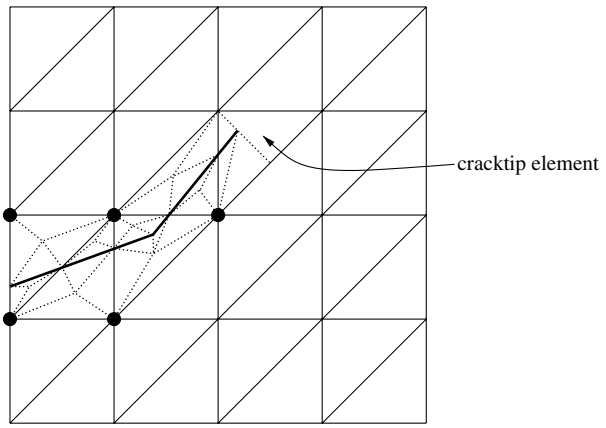

Fig. 3. Enriched nodes (circled) for a two-dimensional structured mesh with three-node triangular elements: partition of elements (dotted lines) for Gauss quadrature is also shown.

2.2. Vector level set method

The Heaviside function $H(\mathbf{x})$ plays a key role in the enriched XFEM displacement field of Eq. 2. Plus, since it needs to be evaluated around the evolving crack-tip, a reliable and efficient procedure to keep track of the crack geometry and to evaluate $H(\mathbf{x})$ is highly desirable.

The level set method (LSM) is a computational technique for modeling a propagating interface. Such an interface is described as the zero level set of a function the dimension of which is higher by one than that of the domain where the interface resides (Osher and Sethian, 1988). Stolarska et al. (2001) first discussed the coupling of the LSM and XFEM and reported that the combination of the two methods is natural and efficient.

Incorporated into our XFEM formulation is an improvement to the original LSM, termed the vector level set method (Ventura et al., 2003), in which the nature of crack propagation problems is fully exploited for enhanced efficiency. The key idea is to restrict the update of the level set function to a small region around the crack-tip, instead of the whole crack, thus eliminating the need to solve partial differential equations to determine the evolution of the entire crack. The level set function at a point $\mathbf{x}$ is described by the sign of the level set function and the components of the closest point projection on the crack, $\mathbf{x}^* - \mathbf{x}$, which are stored only at those nodes that surround the crack. Refer to Ventura et al. (2003) for additional details.

3. Benchmark problem: crack in a plate under uniaxial loading

We use the benchmark problem considered by Huang et al. (2003) to verify the XFEM implementation. In the problem depicted in Fig. 4, a rectangular plate of height $2h = 3$ and width $2b = 2$ is subjected to a uniaxial tensile stress σ. The plate contains, at its center, a crack of length $2a = 0.2$, which is inclined at angle α with respect to the horizontal axis. When $\alpha = 0^\circ$, the state of the crack is very close to the mode I as the size of the crack is small compared with the dimensions of the plate. The mode I stress intensity factor K_I at the crack-tip is

$$K_I = F\left(\frac{a}{b}\right)\sigma\sqrt{\pi a}, \tag{3}$$

where $F(\frac{a}{b})$ is a dimensionless correction factor depending on the ratio $\frac{a}{b}$. For the case of $\frac{a}{b} = 0.1$, $F(\frac{a}{b}) = 1.006$ (Huang et al., 2003).

Both a structured and an unstructured mesh are used in the XFEM numerical simulation. The structured mesh consists of 200×100 triangular elements arranged as in Fig. 3, whereas the unstructured mesh consists of 6032 triangular elements with higher mesh density in the vicinity of the crack. In both cases the mesh density is approximately the same around the crack-tip.

Mode I and mode II stress intensity factors are computed using domain forms of the interaction integrals (Moës et al., 1999). For the area integral to be evaluated, a domain, conveniently assumed to be a circle with radius r_d, needs to be selected with r_d being an arbitrary parameter. The computed SIF values normalized by the theoretical counterparts are listed in Table 1 for a range of r_d used in the domain integral evaluation. It is seen that the SIFs are fairly insensitive to the domain radius, especially when the radius is relatively large, and both the structured and unstructured mesh produce results that are in excellent agreement with theoretical solutions.

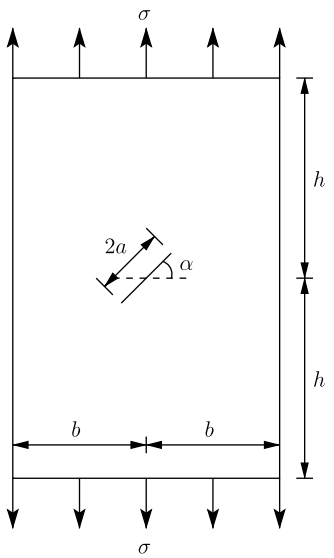

Fig. 4. Plate with an inclined crack under uniaxial tension.

Table 1
Normalized SIFs for the center crack ($\alpha = 0^\circ$)

Structured mesh		Unstructured mesh	
$\frac{r_d}{a}$	$\frac{K_I}{\sigma\sqrt{\pi a}}$	$\frac{r_d}{a}$	$\frac{K_I}{\sigma\sqrt{\pi a}}$
0.245	1.013	0.113	1.013
0.490	0.983	0.226	0.984
0.735	0.990	0.339	0.983
0.980	0.990	0.452	0.980
1.225	0.990	0.565	0.980

When the angle α is greater than 0°, the problem becomes one with a mixed-mode crack and so the mode II (K_{II}) as well as mode I (K_I) SIFs can be assessed. The theoretical solutions for an infinite domain (Anderson, 2005) are

$$K_I = \sigma\sqrt{\pi a}\cos^2\alpha, \quad K_{II} = \sigma\sqrt{\pi a}\sin\alpha\cos\alpha. \tag{4}$$

Listed in Table 2 are the ratios of the calculated to theoretical SIFs for a range of values for α. Very good agreements are obtained again. Accurate assessment of SIFs for a mixed-mode crack is particularly relevant for the present study as such information is crucial in determining the crack growth direction as shown in the next example.

4. Near-interfacial fracture in layered structure

4.1. Experimental evidence in literature

To investigate the capability of the XFEM considered in the present study in the simulation of near-interfacial crack propagation in a layered composite structure, we consider fracture in three-layer ceramic–metal–ceramic structures tested by McNaney et al. (1994). A typical specimen subjected to four-point bending is shown in Fig. 5, where a thin metal layer of thickness h is sandwiched between ceramic materials. The resulting specimen of length L and height W is subjected to a pair of concentrated loads of magnitude P that are distance d apart. A crack of length a, initially parallel to a metal–ceramic interface, exists in the ceramic and propagates upward upon the application of the load.

Experimental as well as theoretical analysis by McNaney et al. (1994) reports that when the crack is situated close to the interface, the crack propagation trajectory is strongly affected by the relative compliance of the two constituent materials for the composite specimen. The crack-tip field of an interfacial crack is affected by Dundurs' parameters α and β (Dundurs, 1969), which describe the effect of the difference in elastic properties of the two constituent materials:

Table 2
SIFs for the inclined crack

α	K_I			K_{II}		
	XFEM	Theory	Ratio	XFEM	Theory	Ratio
15°	0.527	0.523	1.008	0.142	0.140	1.014
30°	0.421	0.420	1.002	0.242	0.243	0.995
45°	0.278	0.280	0.991	0.277	0.280	0.987
60°	0.136	0.140	0.972	0.238	0.243	0.982
75°	0.039	0.038	1.033	0.140	0.140	1.001

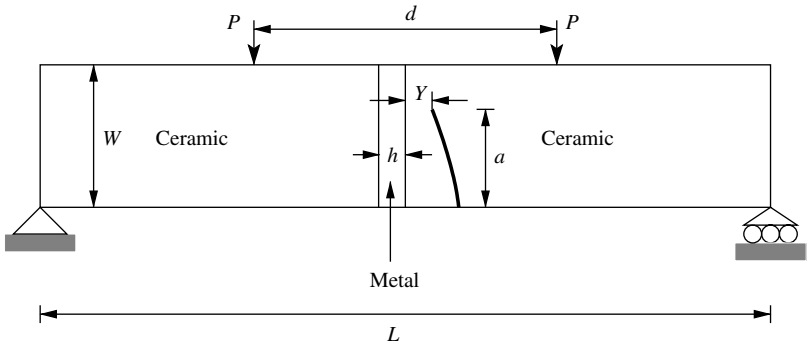

Fig. 5. Four-point bending specimen.

$$\alpha = \frac{E_1' - E_2'}{E_1' + E_2'}, \tag{5}$$

$$\beta = \frac{\mu_1(\kappa_2 - 1) - \mu_2(\kappa_1 - 1)}{\mu_1(\kappa_2 + 1) + \mu_2(\kappa_1 + 1)}, \tag{6}$$

where, for the plane strain loading condition, $E_i' = E_i/(1 - \nu_i^2)$ and $\kappa_i = 3 - 4\nu_i, i = 1, 2$, and E_1, ν_1 and μ_1 (E_2, ν_2 and μ_2) are the Young's modulus, Poisson's ratio and shear modulus of the ceramic (metal), respectively. The study by McNaney et al. (1994) reveals that, for the crack path satisfying the criterion $K_{II} = 0$, the near-interfacial crack is drawn to the interface when $\beta > 0$ while the crack is repelled from the interface when $\beta < 0$.

4.2. Numerical model

XFEM simulations are carried out to numerically replicate the tests that verified such predictions. Two groups of ceramic–metal pairs are considered such that $\beta > 0$ for the alumina/aluminum pair and $\beta < 0$ for the glass/copper pair. Elastic properties and the corresponding Dundurs' parameters for the two groups of material pairs are listed in Table 3. The dimensions of the four-point bending specimen are $L = 25$ mm and $W = 3$ mm for the alumina/aluminum specimen and $L = 30$ mm and $W = 7.5$ mm for the glass/copper specimen. The thickness h of the metal layer is: $50 \sim 100$ μm and 450 μm for aluminum and 125 μm for copper. In all cases, the dimension of the specimen in the out-of-plane direction is 3 mm, and so the plane strain loading condition is assumed.

A typical mesh generated by Triangle (Shewchuk, 2002), a two-dimensional mesh generator and Delaunay triangulator, is depicted in Fig. 6, where a fully developed crack is also shown. A finer mesh density is used in the zone containing the crack

Table 3
Material properties and Dundurs' parameters for two cases of material pairs: alumina/aluminum ($\beta > 0$) and glass/copper ($\beta < 0$)

Material pair 1/2	E_1 (GPa)	ν_1	E_2 (GPa)	ν_2	α	β
Alumina/aluminum	370	0.27	71	0.345	0.666	0.144
Glass/copper	74	0.17	130	0.343	−0.324	−0.183

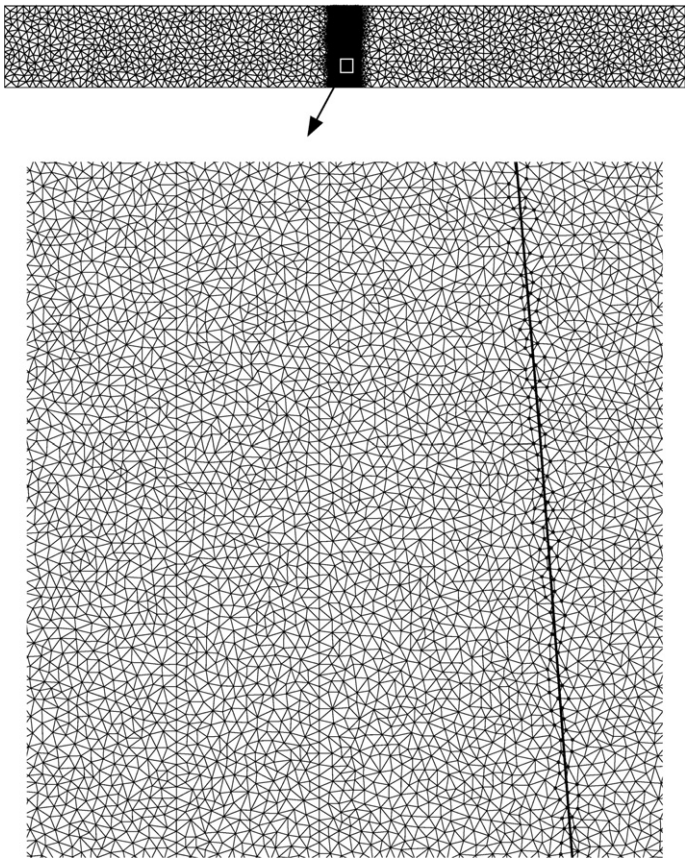

Fig. 6. Mesh for near-interfacial fracture simulation: alumina/aluminum specimen.

as well as the metal layer. The mesh has a symmetric density distribution in the sense that a refinement is provided to both regions that are to the left and right of the metal layer although the region to the right only contains the crack. To improve computational efficiency, meshes with a refined region to the right of the metal layer only have also been used, without any noticeable change in the simulated crack trajectories.

The crack growth direction is determined by the maximum hoop stress criterion (Erdogan and Sih, 1963), which gives the angle of the crack growth

$$\theta_c = 2\arctan\frac{1}{4}\left(\frac{K_I}{K_{II}} \pm \sqrt{\left(\frac{K_I}{K_{II}}\right)^2 + 8}\right), \tag{7}$$

with respect to the local coordinate system for which $\theta_c = 0$ corresponds to the direction of the existing crack. The maximum hoop stress criterion is known to lead to the crack trajectory such that $K_{II} = 0$ (Sukumar and Prévost, 2003).

4.3. Results and discussion

Comparisons of the crack path trajectories simulated by the XFEM with the experimental results obtained by McNaney et al. (1994) are shown in Figs. 7 and 8 (alumina/aluminum; h = 50–100 and 450 μm, respectively) and Fig. 9 (glass/copper; h = 125 μm). In Fig. 7 two groups of XFEM results, one for h = 50 μm and the other for h = 100 μm, are plotted since the experimental results are from specimens for which h was varied from 50 to 100 μm and the actual h for each curve could not be discerned from McNaney et al. (1994). A range of values for the initial distance of the crack from the interface, namely, Y/h at $a/W = 0$ (to be referred to as Y_0/h), are considered to study its influence on the resulting crack trajectory.

In all cases, XFEM simulations correctly capture the important feature of near-interfacial fracture: the crack is drawn to the interface for $\beta > 0$ (Figs. 7 and 8) whereas the crack is deflected away from the interface for $\beta < 0$ (Fig. 9). It is also accurately simulated that the effect of the sign of β on crack trajectories becomes less obvious as Y_0/h increases: Fig. 8 shows that for $Y_0/h \leqslant 1$ the crack is drawn to and ultimately reaches the interface whereas the crack path is less affected by the presence of the metal layer as Y_0/h increases, staying in the ceramic layer until the specimen breaks into two ($a/W = 1$).

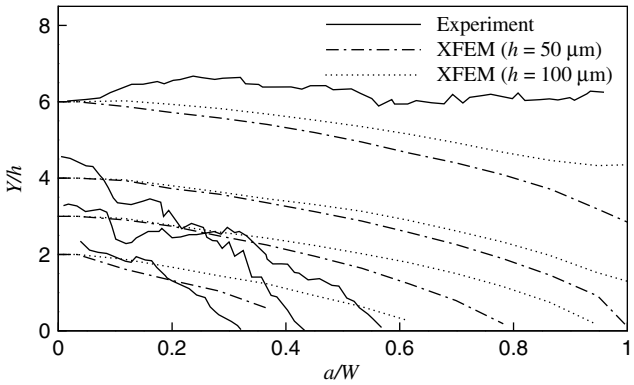

Fig. 7. Comparison of crack trajectories: alumina/aluminum ($\beta > 0$), h = 50—100 μm.

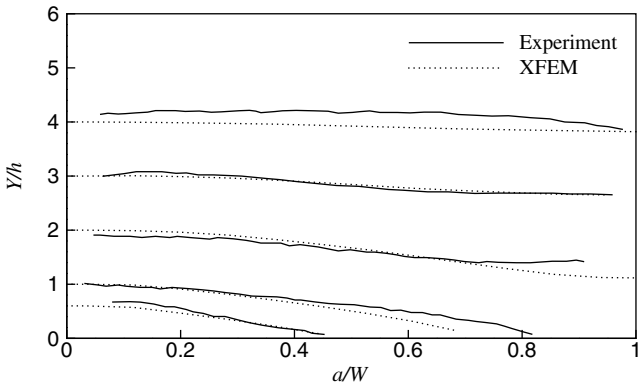

Fig. 8. Comparison of crack trajectories: alumina/aluminum ($\beta > 0$), h = 450 μm.

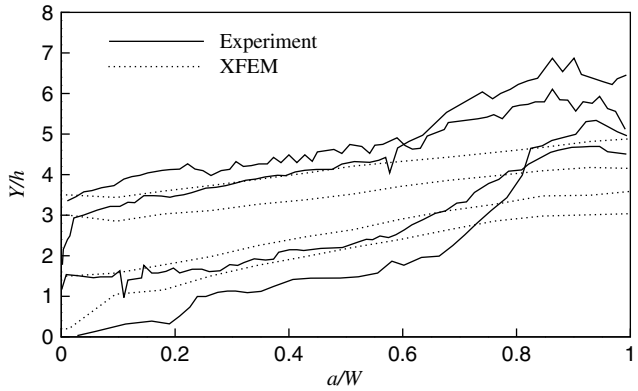

Fig. 9. Comparison of crack trajectories: glass/copper ($\beta < 0$), $h = 125$ μm.

Although qualitative features of the experiment are captured very well by the XFEM, some discrepancies exist as far as exact crack trajectories are concerned. For the purpose of such comparisons, it is first noted that one-to-one comparison of the XFEM and experimental results, as alluded to in Figs. 7–9, may not be justifiable in some cases. This is so because Y_0/h for those cases cannot be clearly identified from the drawings provided in McNaney et al. (1994). Nevertheless, care was exercised in the XFEM simulation to ensure that Y_0/h would be comparable for simulations and experiments.

For the alumina/aluminum specimen with $h = 450$ μm (Fig. 8), the simulated crack trajectories are in excellent agreement with the test results for a wide range of Y_0/h. On the other hand, the degree of agreement for $h = 50$–100 μm depends on Y_0/h (Fig. 7). For each value of Y_0/h the two trajectories obtained by the XFEM, one for $h = 50$ μm and the other for 100 μm, provide an envelope, within which a trajectory corresponding to the experimental one exists. It is noted that, in the case of $Y_0/h \approx 2$ and 3, the simulated trajectories for $h = 50$ μm are relatively close to the experimental ones while the crack path for $h = 100$ μm more closely follows the experimental result in the case of $Y_0/h \approx 6$. The envelope for $Y_0/h \approx 4$, however, does not embrace the test result with comparable accuracy. It is also observed that the experimental curves for $Y_0/h \approx 3$ and 4 intersect with each other, which may be a clear sign that different h's were used for those cases. Intersecting crack trajectories can also be simulated by the XFEM as illustrated in Fig. 10, albeit with a different combination of Y_0/h and h.

In the case of the glass/copper specimen (Fig. 9), the simulated trajectories are quite close to the experimental ones especially when the crack is still in its early stage of growth. Discrepancies become larger as the crack is fully developed with an increased rate of departure from the interface. In contrast, the simulated paths are seen to be deflected away from the interface with approximately a constant slope. However, test results involve intersecting curves, which suggests that the accelerated departure of the cracks in some cases may be misrepresenting the true behavior.

The influence of the mesh density on crack trajectories is also investigated by considering three increasingly refined meshes for the zone where the crack resides. The area of the elements for the coarsest mesh is 200 μm^2, and the area is reduced by a factor of four from one level of refinement to the next. In the case of the alumina/aluminum specimen with $h = 100$ μm, the results shown in Fig. 11 indicate that the mesh density has relatively insignificant influences. For some values of Y_0/h, the cracks due to a finer mesh are drawn to the interface slightly faster, being closer to the experimental results.

The foregoing discussion indicates that overall comparisons of computational and experimental results are deemed very good. Nevertheless, it is expected that improvements can be attained by introducing additional ingredients into the numer-

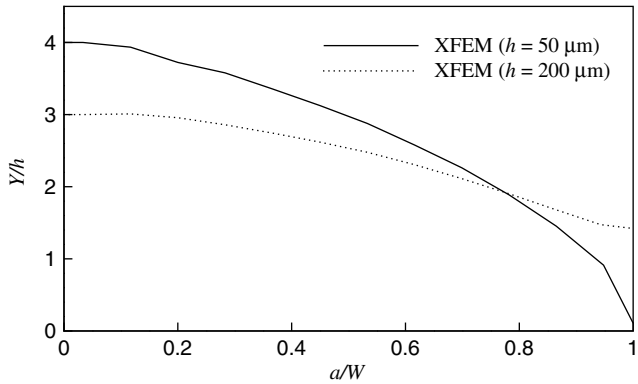

Fig. 10. Intersection of simulated crack trajectories: alumina/aluminum ($\beta > 0$), $h = 50$ and 200 μm.

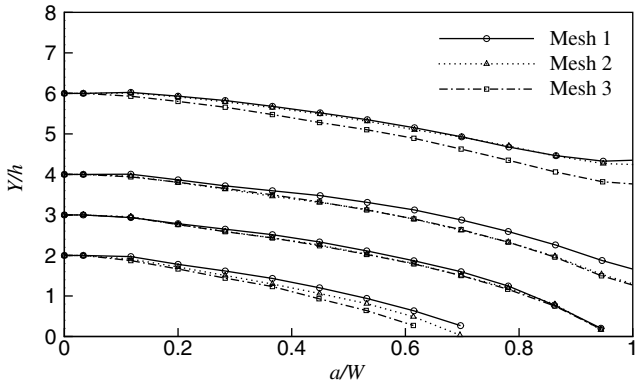

Fig. 11. Influence of the mesh density on crack trajectories: alumina/aluminum ($\beta > 0$), $h = 100\ \mu m$. The area of elements in the zone where the crack resides is 200, 50 and 12.5 μm^2 for mesh 1, 2 and 3, respectively.

ical model. First, the simulation entails complete breakage of specimens ($a/W = 1$), for which consideration of large deformation may be necessary. By the same token, plasticity of the metal may have affected the displacement field around the crack. While pure brittle cracking was assumed in the present study for a crack initiation criterion, use of a proper cohesive crack model is expected to more closely capture the fracture behavior of alumina as evidenced by experiments (Llorca and Steinbrech, 1991). Use of higher-order elements that allows for a better kinematic representation of the crack geometry as well as the finite-element displacement field may enhance the comparison further.

5. Concluding remarks

An XFEM relying on Heaviside enrichment only has been applied to the analysis of near-interfacial fracture in ceramic-metal–ceramic layered structures. The method accurately captures the important aspect of the fracture behavior that the crack growth trajectory is either drawn to or repelled from the ceramic–metal interface depending on the relative elastic properties of the constituent materials. The crack path observed in experiments are also closely reproduced by XFEM simulations. It is expected that some observed discrepancies in crack paths may be reduced by considering inelastic behavior of the structure as well as higher-order kinematic descriptions in the XFEM formulations. Incorporation of such additional modeling capabilities are the subject of future studies. The modeling capability demonstrated in this study indicates that the XFEM may adequately tackle more involved problems in near-interfacial fracture.

Acknowledgments

The authors wish to thank the Innovative Bridge Research and Construction (IBRC) Program of the US Federal Highway Administration for supporting the research reported in this paper.

References

Anderson, T.L., 2005. Fracture Mechanics: Fundamentals and Applications. Taylor and Francis Group, Boca Raton, FL.
Büyüköztürk, O., Gunes, O., Karaca, E., 2004. Progress on understanding debonding problems in reinforced concrete and steel members strengthened using FRP composites. Construction and Building Materials 18, 9–19.
Camata, G., Spacone, E., Zarnic, R., 2007. Experimental and nonlinear finite element studies of RC beams strengthened with FRP plates. Composites: Part B: Engineering 38, 277–288.
Chen, H., 2003. Enriched finite element methods and their application. Ph.D thesis, Northwestern University, Evanston, IL.
Chen, J.F., Teng, J.G., 2003. Shear capacity of FRP-strengthened RC beams: FRP debonding. Construction and Building Materials 17, 27–41.
Chessa, J., Wang, H., Belytschko, T., 2003. On the construction of blending elements for local partition of unity enriched finite elements. International Journal for Numerical Methods in Engineering 57, 1015–1038.
Dundurs, J., 1969. Discussion of edge-bonded dissimilar orthogonal elastic wedges under normal and shear loading. Journal of Applied Mechanics 36, 650–652.
Erdogan, F., Sih, G., 1963. On the crack extension in plates under plane loading and transverse shear. Journal of Basic Engineering 85, 519–527.
Huang, R., Sukumar, N., Prévost, J.-H., 2003. Modeling quasi-static crack growth with the extended finite element method. Part II. Numerical applications. International Journal of Solids and Structures 40, 7539–7552.
Jirásek, M., 2000. Comparative study on finite elements with embedded discontinuities. Computer Methods in Applied Mechanics and Engineering 188, 307–330.
Jirásek, M., Belytschko, T., 2002. Computational resolution of strong discontinuities. In: Mang, H., Rammerstorfer, F., Eberhardsteiner, J. (Eds.), Fifth World Congress on Computational Mechanics. Vienna, Austria.
Leung, C.K.Y., 2006. FRP debonding from a concrete substrate: some recent findings against conventional belief. Cement and Concrete Composites 28, 742–748.
Llorca, J., Steinbrech, R.W., 1991. Fracture of alumina: an experimental and numerical study. Journal of Materials Science 26, 6383–6390.
McNaney, J.M., Cannon, R.M., Ritchie, R.O., 1994. Near-interfacial crack trajectories in metal–ceramic layered structures. International Journal of Fracture 66, 227–240.

Melenk, J.M., Babuška, I., 1996. The partition of unity finite element method: basic theory and applications. Computer Methods in Applied Mechanics and Engineering 139, 289–314.
Moës, N., Dolbow, J., Belytschko, T., 1999. A finite element method for crack growth without remeshing. International Journal for Numerical Methods in Engineering 46, 131–150.
Ngo, D., Scordelis, A.C., 1967. Finite element analysis of reinforced concrete beams. Journal of American Concrete Institute 64, 152–163.
Osher, S., Sethian, J.A., 1988. Fronts propagating with curvature dependent speed: algorithms based on Hamilton–Jacobi formulations. Journal of Computational Physics 79, 12–49.
Shewchuk, J.R., 2002. Delaunay refinement algorithms for triangular mesh generation. Computational Geometry: Theory and Applications 22, 21–74.
Simo, J.C., Oliver, J., Armero, F., 1993. An analysis of strong discontinuities induced by strain-softening in rate-independent inelastic solids. Computational Mechanics 12, 277–296.
Stolarska, M., Chopp, D.L., Moës, N., Belytschko, T., 2001. Modeling crack growth by level sets in the extended finite element method. International Journal for Numerical Methods in Engineering 51, 943–960.
Sukumar, N., Huang, Z.Y., Prévost, J.-H., Suo, Z., 2004. Partition of unity enrichment for bimaterial interface cracks. International Journal for Numerical Methods in Engineering 59, 1075–1102.
Sukumar, N., Prévost, J.-H., 2003. Modeling quasi-static crack growth with the extended finite element method. Part I. Computer implementation. International Journal of Solids and Structures 40, 7512–7537.
Triantafillou, T.C., Antonopoulos, C.P., 2000. Design of concrete flexural members strengthened in shear with FRP. Journal of Composites for Construction 4 (4), 198–205.
Ventura, G., Budyn, E., Belytschko, T., 2003. Vector level sets for description of propagating cracks in finite elements. International Journal for Numerical Methods in Engineering 58, 1571–1592.
Zi, G., Belytschko, T., 2003. New crack-tip elements for XFEM and applications to cohesive cracks. International Journal for Numerical Methods in Engineering 57, 2221–2240.